OPEN ACCESS

Modeling of two-dimensional nanoscale Y-bent plasmonic waveguides with cavities for demultiplexing of the telecommunication wavelengths

New Journal of Physics
The open-access journal for physics

Modeling of two-dimensional nanoscale Y-bent plasmonic waveguides with cavities for demultiplexing of the telecommunication wavelengths

A Noual, A Akjouj[1], Y Pennec, J-N Gillet and B Djafari-Rouhani
Institut d'Electronique, de Microélectronique et de Nanotechnologie, UMR CNRS 8520, Université de Lille 1, 59655 Villeneuve d'Ascq, France
E-mail: Abdellatif.Akjouj@univ-lille1.fr

New Journal of Physics **11** (2009) 103020 (19pp)
Received 31 July 2009
Published 7 October 2009
Online at http://www.njp.org/
doi:10.1088/1367-2630/11/10/103020

Abstract. Numerical simulations, based on a finite-difference-time-domain (FDTD) method, of infrared light propagation for add/drop filtering in two-dimensional (2D) metal–insulator–metal (Ag–SiO_2–Ag) resonators are reported to design 2D Y-bent plasmonic waveguides with possible applications in telecommunication wavelength demultiplexing (WDM). First, we study optical transmission and reflection of a nanoscale SiO_2 waveguide coupled to a nanocavity of the same insulator located either inside or on the side of a linear waveguide sandwiched between Ag. According to the inside or outside positioning of the nanocavity with respect to the waveguide, the transmission spectrum displays peaks or dips, respectively, which occur at the same central frequency. A fundamental study of the possible cavity modes in the near-infrared frequency band is also given. These filtering properties are then exploited to propose a nanoscale demultiplexer based on a Y-shaped plasmonic waveguide for separation of two different wavelengths, in selection or rejection, from an input broadband signal around 1550 nm. We detail coupling of the 2D add/drop Y connector to two cavities inserted on each of its branches. Selection or rejection of a pair of different wavelengths depends on the inside or outside locations (respectively) of each cavity in the Y plasmonic device.

[1] Author to whom any correspondence should be addressed.

Contents

1. Introduction

Electromagnetic waves coupled to propagating free electron oscillations at metal–insulator–metal (MIM) interfaces, known as surface plasmons polaritons (SPPs), have been considered as energy and information carriers to significantly overcome the classical diffraction limit [1]. For example, light energy localization in volumes as tiny as 0.001 λ^3 (where λ is the vacuum wavelength) was obtained with a 3 nm-thick plasmonic nanosheet in an experimental study [2]. A number of plasmonic waveguiding structures have been proposed such as metallic strips and nanowires [3, 4] as well as V and W grooves in metal substrates [5]–[8], plasmon slots [9, 10], ring resonators [11] and metal wedges [12]–[15]. Among these structures, those focusing light into the dielectric core in a MIM setup allow manipulation and transmission of signals at the nanoscale. MIM-based plasmon-slot waveguides have therefore been used to provide both long-range propagation and sub-wavelength spatial confinement [9, 16]. MIM waveguides are promising for the design of nanoscale all-optical devices owing to strong localization and zero bend loss with a relatively easy fabrication according to the current state of the art [17]–[19]. These plasmonic nanostructures were applied to the design of switches [20], sub-wavelength imaging systems [21], thermal emitters and biosensors [22], and dye enhancers for organic compounds [23], for instance. Moreover, broad-bandgap MIM waveguides with low side lobes were proposed as an alternative to fiber Bragg gratings for fibered telecommunications [24]. Metallic plasmonic slits were used for the design of Terahertz devices with near-field applications [25]. Far-field radiations were also obtained using nano-antennas designed from plasmonic dipolar emitters [26, 27].

In this paper, we investigate the filtering properties of nanocavity resonators in a two-dimensional (2D) plasmonic waveguide around 1.5 μm with Ag–SiO_2–Ag interfaces using a finite-difference-time-domain (FDTD) method [28] and perfectly matched-layer (PML) boundary conditions. The physical effect of coupling the nanowaveguide to a cavity is to induce peaks or dips (zeros) in the transmission coefficient depending on the inside or outside cavity location (respectively) compared with the SiO_2 waveguide. We detail the possibility of a selective peak or rejective dip in the transmission from an appropriate choice of the geometrical parameters of the structure. These filtering cavities are then exploited to show the possible design of a novel nanoscale plasmonic device (to our knowledge) for wavelength demultiplexing (WDM) in add/drop telecommunication using a 2D Y-bent plasmonic component.

This paper is organized as follows. In section 2, we present briefly the FDTD method. Sections 3 and 4 study the structures presenting selective (add) and rejective (drop) plasmonic waveguide respectively. The Y-bent add/drop plasmonic waveguide is discussed in section 5.

Finally, some conclusions regarding the filtering and demultiplexing in nanoscale plasmonic waveguides are drawn in section 6.

2. Numerical method

In our numerical calculations with FDTD, the nanocavity resonator is described by a spatial discretisation grid. Similarly to preceding works [29], a spatial grid size of $\Delta x = \Delta y = 4\,\text{nm}$ in the FDTD algorithm was found to be sufficient for convergence of the numerical results. Calculations are performed by replacing partial derivatives in the Maxwell equations by finite differences. Our system is made up of a 2D box (along x- and y-axes) with propagation along the y-axis. PML boundary conditions are applied at both boundaries in y and x of the box in order to eliminate the reflection of outgoing waves [30, 31]. The PML width of 160 nm was found to be thick enough to fully absorb outgoing waves. The structure is supposed to be infinite along the z-direction. The equations of motion are solved with a time integration step $\Delta t = (\Delta x \times 0.25/c) = 3 \times 10^{-3}\,\text{fs}$ and number of time steps equal to 2^{20}, which is the necessary tested time for good convergence of the numerical calculations. The chosen metal in our simulations is Ag since it absorbs less energy in the telecommunication range (around 1.55 μm) comparing with other metals (Au, for instance).

The dielectric function of the metal is described by the lossy Drude model

$$\varepsilon(\omega) = \varepsilon_\infty - \omega_p^2/(\omega^2 + i\Gamma\omega), \tag{1}$$

where ε_∞ is the relative permittivity at an infinite frequency, ω_p is the plasma frequency and Γ is the collision frequency. We use $\varepsilon_\infty = 3.276$, $\omega_p = 1.38 \times 10^{16}\,\text{rad}\,\text{s}^{-1}$ and $\Gamma = 2.634 \times 10^{13}\,\text{rad}\,\text{s}^{-1}$ for the Drude model, which fit the experimental data with a low error in the near-infrared spectrum [32]. The waveguide width of 50 nm is 31 folds smaller than the wavelength of the incident signal in vacuum (figure 1(a)). According to the symmetry of the perfect waveguide, the propagating waves can be distinguished between symmetric and antisymmetric SPP modes [33]. Figure 1(a) presents the dispersion relation of SPP modes in a silicon dioxide slab sandwiched between two semi-infinite parts made up of Ag. The dimensionless frequency (ω/ω_p) is plotted versus the reduced wave vector ($k_{||}d$). In figure 1(a), we assume that $k_{||}$ is the wave vector parallel to the waveguide, $\varepsilon_2 = 2.28$ is the dielectric constant of SiO_2 and $\varepsilon_1 = \varepsilon_1(\omega)$ is the dielectric constant of the silver metal (given by the Drude model). The width of the waveguide is denoted by d. c is the light velocity in vacuum. The two dispersion curves '1' and '2' correspond to modes confined in the dielectric region and decaying exponentially on both sides into the interior of the metal. These modes result in interaction of each interface (SiO_2/Ag) SPP mode of the structure. Degeneracy suppression leads to symmetric (branch 2) and antisymmetric (branch 1) modes. Both branches have transverse-magnetic (TM) polarization, which means that the magnetic field is perpendicular to the wave propagation direction and the symmetry of the modes is defined with respect to the plane symmetry of the structure. In this work, the antisymmetric mode, for which the waveguide is monomode in a large reduced frequency range from 0.06 to 0.136, is only excited. This range corresponds to the near-infrared wavelength range from 1000 to 2400 nm in vacuum. In figure 1(b), the magnetic field profile is presented in the plane (x, z) for $\lambda = 1550\,\text{nm}$ (in vacuum). From this curve, the skin depth at this wavelength is estimated as $\delta = 44\,\text{nm}$.

The incoming pulse is generated at the left end of the structure (inset in figure 2(a)) inside the taper region, by a current source parallel to the x-axis and having a Gaussian profile along

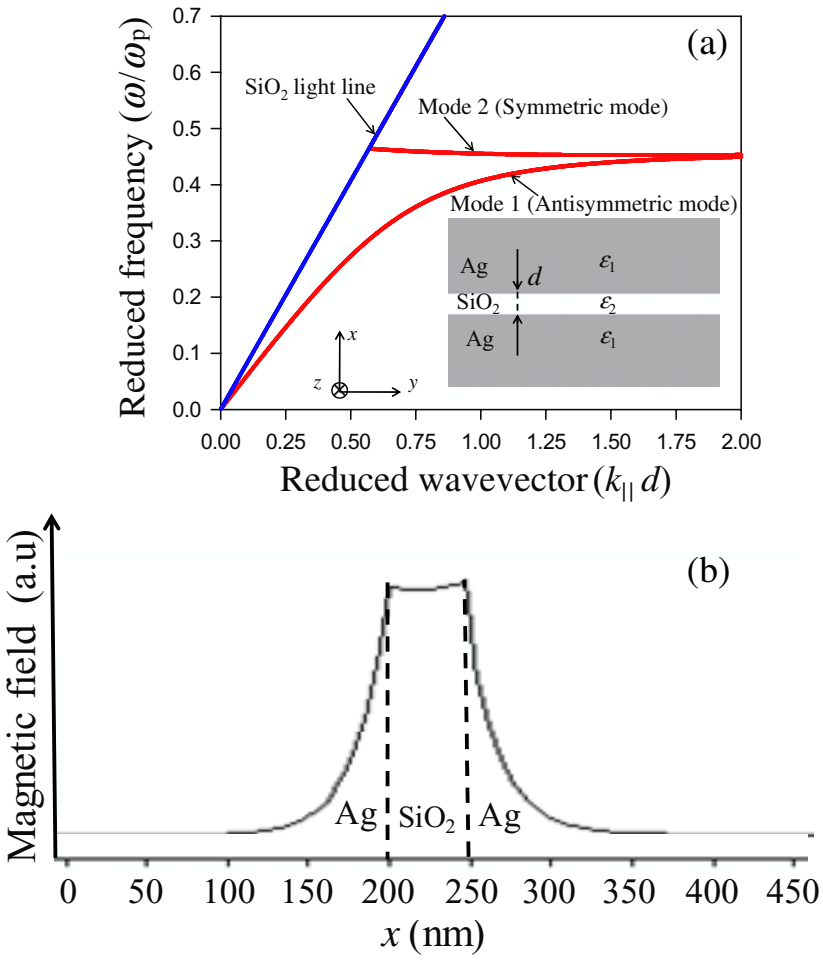

Figure 1. (a) Dispersion relation (reduced frequency versus reduced wave vector) for an Ag–SiO_2–Ag planar waveguide with the structure in the inset. The width of the waveguide is denoted by $d = 50$ nm while ε_2 and ε_1 from the Drude model are the dielectric parameters of SiO_2 and Ag, respectively. (b) Magnetic-field penetration profile with a skin depth δ on the (x, z)-plane with $y = \text{const}$.

the x-direction. The configuration of the current source (J_x) according to the plane symmetry of the waveguide is antisymmetric, which allows excitation of the antisymmetric mode. The current is generated during a short period of time for excitation of the electromagnetic waves in the telecommunication frequency domain. The transmitted signal, probed at the right end of the waveguide, is recorded as a function of time, integrated over the cross section of the waveguide and finally Fourier transformed to obtain the transmission coefficient versus the wavelength. The excited signal covers the telecommunication wavelength range from 1300 to 1730 nm in vacuum. The coupling loss between the light source and waveguide is estimated as low as 6 dB. All transmission spectra are normalized with respect to that corresponding to a bare waveguide (without nanocavity resonator). The transmission is reported in decibel (dB) as a function of the wavelength (nm) of the light in air.

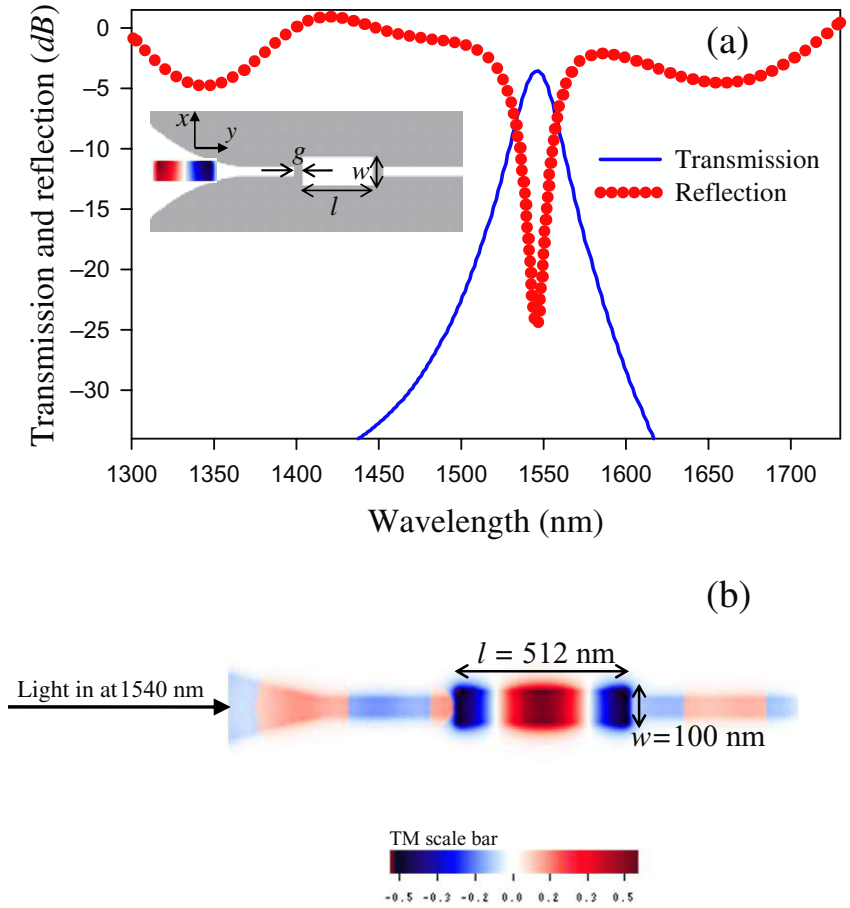

Figure 2. (a) Transmission (solid line) and reflection (dotted line) spectra versus wavelength in vacuum (nm) for the system in the figure inset with the inside-cavity parameters $l = 512\,\text{nm}$ (length), $w = 100\,\text{nm}$ (width) and $g = 20\,\text{nm}$ (metallic gap). Both transmission and reflection are normalized with respect to the output and input powers of the straight waveguide without cavity. Inset: Ag–SiO_2–Ag structure with a rectangular nanocavity inside the waveguide. (b) Magnetic-field map (TM) for a monochromatic incident signal at the wavelength of the transmission maximum ($\lambda = 1540\,\text{nm}$).

3. Selective plasmonic sub-waveguide

The inset in figure 2(a) shows the geometry of the structure, which is constituted of a rectangular resonator cavity located in the interior of a bus waveguide. The cavity is made up of one piece of SiO_2 separated from the rest of the main guide by two thin pieces of Ag metal. Coupling between the cavity resonator and input waveguide depends on the thickness g of the metallic gap between the sketched pieces of Ag metal. According to the skin depth value of ∼44 nm, the g-value should be less than 44 nm. l and w are, respectively, the length and width of the cavity. The embedding medium is Ag. We refer to the cavity resonator dimensions by the 2-tuple (w, l) with both values given in nanometers.

In figure 2(a), we present the calculated transmission (solid line) and reflection (dashed line) spectra as a function of the wavelength for a nanocavity resonator inserted inside the waveguide with $l = 512$ nm, $w = 100$ nm and $g = 20$ nm. Such a cavity possesses several SPP modes, whose number and positions depend on the cavity aspect ratio and volume as well as the surrounding medium permittivity [34]. For the presented structure, only one resonance appears in the computed wavelength range, as shown in figure 2(a). Interaction between the linear waveguide and nanocavity through the two metallic pieces forms a narrow peak in the transmission spectrum for the telecommunication wavelengths around 1540 nm (figure 2(a)), resulting in a selective filter. The reflection coefficient evaluated at the entrance of the waveguide falls down to 13% while the transmission is about 63% (−5 dB). This means that approximately 24% of the input signal has been absorbed inside the cavity. These estimations are not significantly altered by absorption during propagation along the waveguide. Indeed, attenuation can be evaluated as only $-0.5\,\mathrm{dB}\,\mu\mathrm{m}^{-1}$. The peak in the transmission spectrum appears at the wavelength of the SPP eigenmode (i.e. the resonance) of the cavity. The latter is calculated in the following way: a transient pulse is first generated in an isolated cavity inside a thick metal. Then, the TM field is probed at different positions in the cavity during the simulation time. A Fourier transform of the transient response is finally computed to obtain the frequency spectrum.

The map corresponding to the magnetic field for the resonance mode ($\lambda = 1540$ nm) is shown in figure 2(b). We notice a strong interaction between the waveguide and cavity, leading to excitation of a SPP mode localized at the boundaries and in the middle of the cavity. This interaction induces transmission and absorption of the resonant wavelength. Nevertheless, all other wavelengths of the broadband signal are reflected as displayed in the reflection coefficient in figure 2(a). The same phenomenon of exaltation of the output transmission of a discrete energy mode localized in a cavity between two potential barriers is usual in quantum mechanics. A traditional example is the tunneling of discrete energy levels in a quantum well through double barriers [35]. Another example is the tunneling of discrete energy levels through a quantum dot, leading to oscillations in its electronic transport properties as its electrical conductivity [36]. In the proposed selection cavity, we show that an analogue tunneling effect is possible in classical electrodynamics since a unique cavity plasmonic eigenmode is localized between double Ag barriers for the considered broadband wavelength range. In figure 2(b), we also point out that the magnetic-field (eigenvector) is antisymmetric with respect to the axis parallel to the large side of the cavity as well as that parallel to the small side of the cavity.

In figures 3(a) and (b), the variation of the wavelengths corresponding to the cavity eigenmode and peak in the transmission coefficient is studied as a function of the geometrical parameters l and w of the cavity. Remind that the interaction between the antisymmetric mode of the waveguide and plasmon mode of the cavity through the two pieces of metal displays a transmission peak with an amplitude of 63% (−5 dB). In figure 3(a), the transmission coefficient is calculated for different lengths $l = 480$, 500, 512, 520 and 540 nm of the cavity when the width w is taken equal to 100 nm. We observe that increasing the cavity length l shifts the resonant mode to the higher wavelengths. Figure 3(b) presents the transmission spectrum for different values of $w = 80$, 100, 120, 140 and 160 nm, the constant length l being equal to 512 nm. Unlike the previous case, the increase in the cavity width w shifts the mode to lower wavelengths although the variation in the resonance wavelength is weaker than that in figure 3(a). The quality factor Q of the selected peaks (resonance wavelengths) reaches the high value of 130. Q is defined by the following equation: $Q = \lambda_r/\Delta\lambda$, where λ_r is the resonant wavelength and the bandwidth $\Delta\lambda$ is the full width at half maximum. The higher values of the

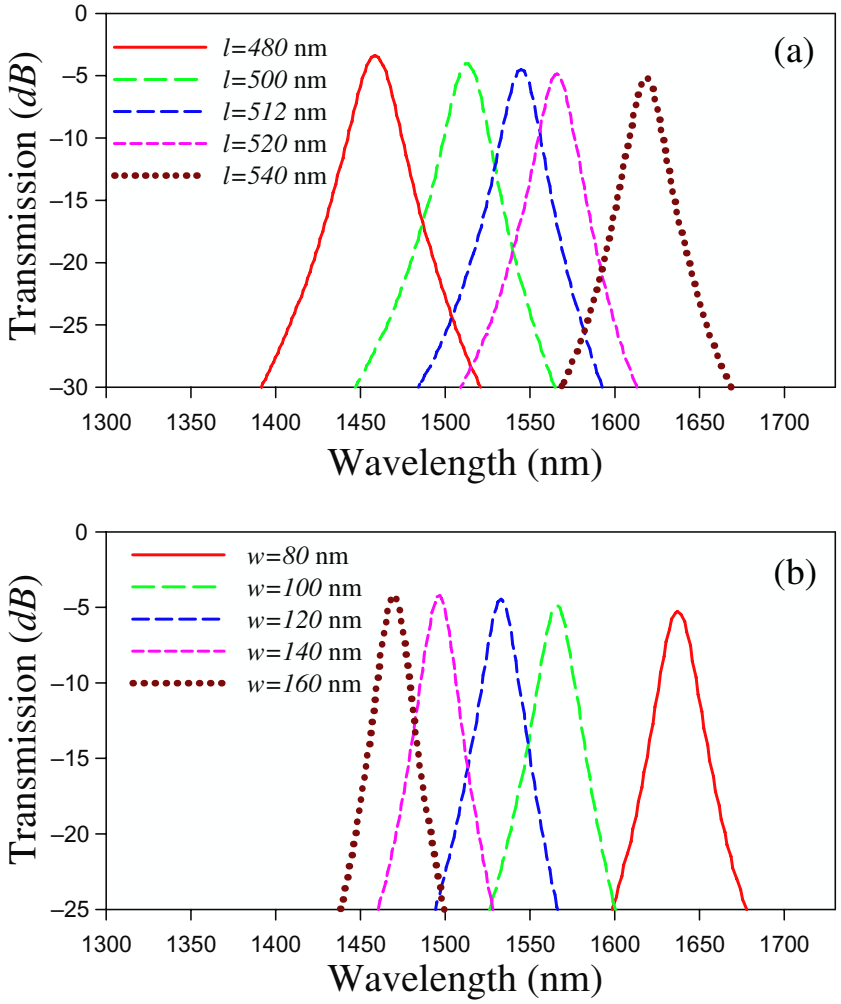

Figure 3. (a) Shift of the transmitted peak as function of the wavelength for different values of the cavity length l with constant $w = 100$ nm and $g = 20$ nm. (b) Similar diagram than that in (a) but for a variable cavity width w with constant $l = 512$ nm and $g = 20$ nm.

quality factor are obtained by increasing the thickness of the two thin pieces of metal (metallic gap g) that separate the cavity from the linear waveguide. The preceding result is strongly correlated to a weaker coupling between the cavities and waveguide. However, the thickness g should not exceed 44 nm (according to the estimated skin depth δ). Otherwise, coupling between the cavity and waveguide is not sufficient to induce signal peaks with a high energy transmission rate. Improvement of the Q-factor relies on an accurate fabrication of the device.

Figures 4(a) and (b) show, respectively, the evolution of the resonance wavelengths versus the length l and width w of the cavity. We notice the linear increase of the λ versus l curve and nonlinear decrease of that of λ versus w. This observation is the opposite with respect to the usual behavior of a photonic cavity in which the increase of both dimensions l and w leads to a linear increase of the resonance wavelength. A similar evolution of the resonance wavelength with respect to the cavity size parameters ($\lambda \sim l$ for const. w and $\lambda \sim 1/w$ for const. l) was also obtained and analyzed when the air cavity is located on the side of the air waveguide [37, 38].

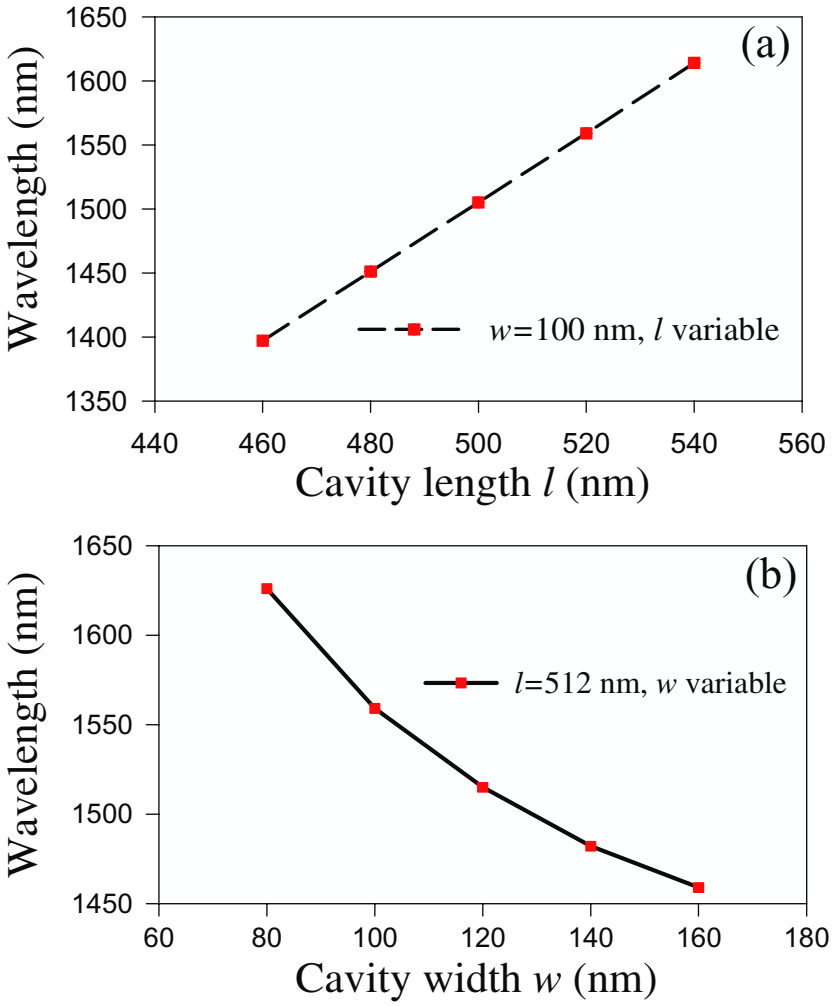

Figure 4. (a) Transmitted-peak wavelength versus cavity length l with constant $w = 100$ nm and $g = 20$ nm. (b) Similar diagram than that in (a) but for a variable cavity width w with constant $l = 512$ nm and $g = 20$ nm.

We further observe an additional slight shift of the resonance wavelength when the metallic gap g is modified. Finally, note that we can precisely tune the selected resonance wavelength λ in a broadband range by changing the device size parameters as the width w or length l of the cavity.

4. Rejection plasmonic sub-waveguide

In this section, we consider another type of cavity located on the side of the SiO_2 waveguide. It is well known that the coupling of a waveguide to a side resonator can give rise to the excitation of the latter at its resonance frequency and, as a consequence of interference phenomena, produce a dip in the transmission spectrum at this specific frequency. In our structure, the cavity is made up of one rectangular piece of SiO_2 that is, however, separated from the waveguide by a metallic gap of thickness g (inset in figure 5(a)). The corresponding transmission and reflection spectra are presented in figure 5(a) with the following parameters: $w = 100$ nm, $l = 512$ nm and

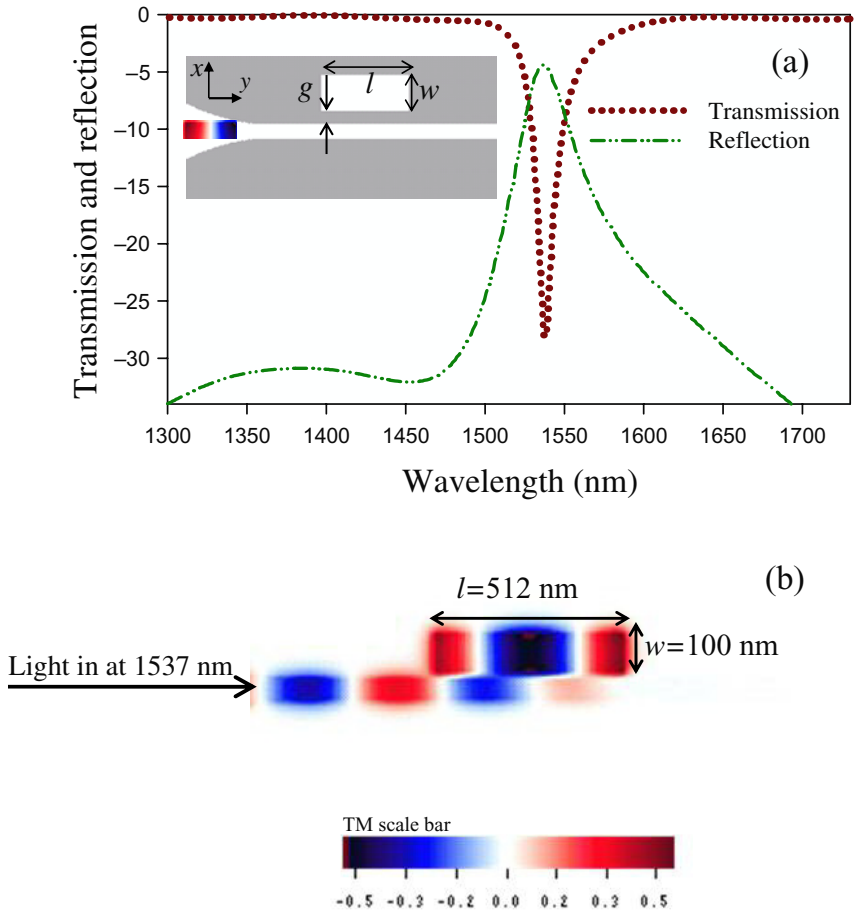

Figure 5. (a) Transmission (dotted line) and reflection (dashed-dotted line) spectra versus wavelength in vacuum (nm) for the system in the figure inset with the outside-cavity parameters $l = 512\,\text{nm}$, $w = 100\,\text{nm}$ and $g = 32\,\text{nm}$. Inset: Ag–SiO_2–Ag structure with a rectangular nanocavity outside the waveguide. (b) Magnetic-field map (TM) for a monochromatic incident signal at the wavelength of the zero of transmission ($\lambda = 1537\,\text{nm}$).

$g = 32\,\text{nm}$. We observe that all wavelengths are transmitted except that associated to excitation of the cavity SPP mode. The wavelength of the resonance mode, equal to 1540 nm, is the same as that obtained in the preceding section for a transmission peak when the cavity is located inside the waveguide. Indeed, the outside cavity has the same size parameters than that located inside the bus waveguide in section 3. However, the electromagnetic energy associated to this cavity eigenmode is localized in the outside cavity with no possibility of tunneling with respect to the longitudinal axis y of the bus waveguide, leading to a dip in the output energy spectrum for the resonance wavelength. The equality between the resonance frequencies of the peak and of the dip in the transmission spectrum, depending on whether the cavity is positioned inside or outside of the waveguide, was first demonstrated in the case of a waveguide inside a phononic crystal [39]. These localization effects allow us to design a rejection filter in the telecommunication range. Our FDTD calculations confirm us that interaction between the waveguide and nanocavity through the metallic gap forms a significant dip of $-30\,\text{dB}$ in the

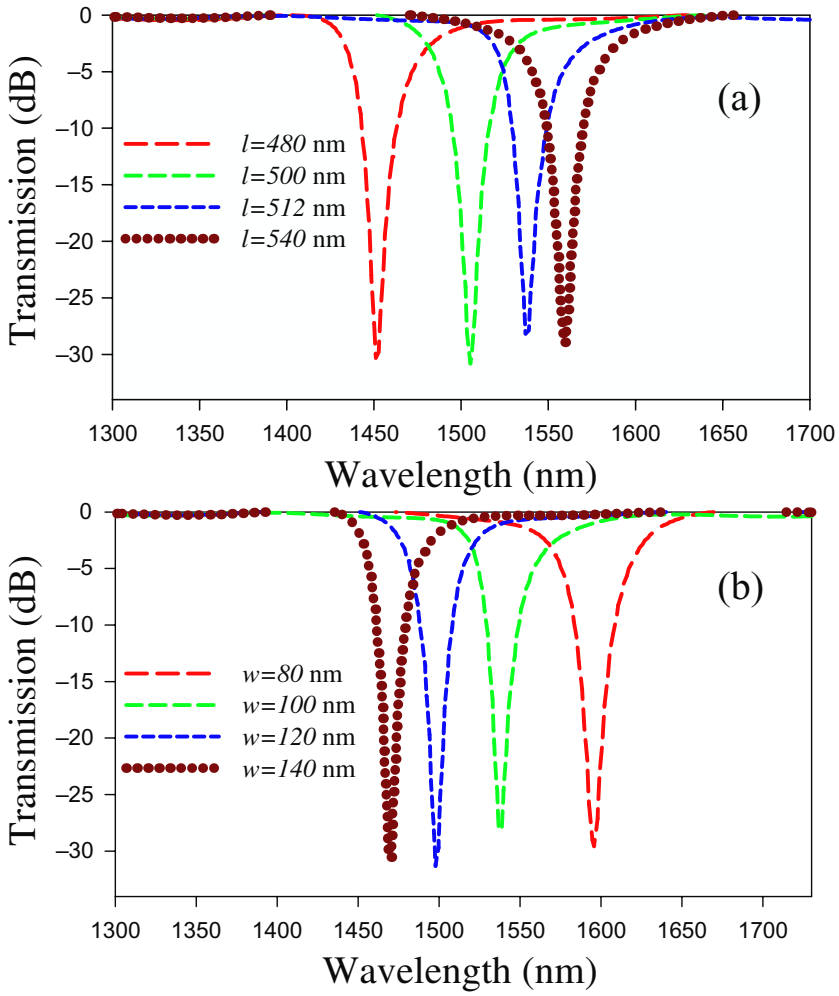

Figure 6. (a) Shift of the zero of the transmission spectrum versus wavelength for different values of the cavity length l with constant $w = 100$ nm and $g = 32$ nm. (b) Similar diagram than that in (a) but for a variable cavity width w with constant $l = 512$ nm and $g = 32$ nm showing an opposite effect.

transmission spectrum at the resonance wavelength (figure 5(a)). Indeed, only a small amount of the localized energy associated to the eigenmode can escape the cavity through the metallic gap. The reflection coefficient, computed at the entrance of the waveguide, has a low db value of −5 dB (i.e. 64%), which means that approximately 36% of the input signal is absorbed inside the cavity. The TM field map of the reflected mode is shown in figure 5(b). We observe a strong interaction between the waveguide and nanocavity, leading to important localization effects. The symmetry of the cavity eigenmode is the same as that in figure 2(b).

Evolution of the reflected wavelength versus the geometrical parameters is studied in figure 6. In (a), the transmission coefficient is given for different cavity lengths l (with $l = 480$, 500, 512 and 520 nm) when the constant width w is equal to 100 nm. As in section 3, we notice the shift of this mode to higher wavelengths after increase of the cavity length l. Figure 6(b) shows the transmission spectrum for different values of $w = 80$, 100, 120 and 140 nm with a

constant length l equal to 512 nm. Unlike the preceding case, the increase of the outside-cavity width shifts the mode to lower wavelengths although the variation in the resonance wavelength is weaker than that in figure 6(a). These trends show a good agreement with those presented in figure 3. As in the case of a selective filter (inside cavity), the quality factor Q takes higher values by increasing the thickness of the metallic gap g of the rejection filter. Q reaches the value of 153. This Q-value is slightly higher than that obtained for the selective filter. This increase comes from a weaker coupling with the waveguide through the metallic gap when the cavity is outside of the waveguide.

We also analyze the transmission and reflection spectra when the linear waveguide interferes with a pair of outside SiO_2 nanocavities showing the same size parameters as well as mirror symmetry with respect to the central in-plane section of the bus waveguide. When the dimensions of both cavities are 512 nm for their length l, 100 nm for their width w and 32 nm for their metallic gap g, we obtain a transmission dip with the same resonance frequency as that of the single cavity. However, this dip presents a better isolation with a db value reduced to -41 dB. If g is augmented to 40 nm, we obtain an even higher quality factor $Q = 172$ corresponding to an increase of 12% compared with a single cavity. However, the stopped band remains isolated with a dip at -29 dB. For specific telecommunication applications requiring a high quality factor and low dip of at least -30 dB in the transmission spectrum, it might be even better to use a pair of nanocavities around the linear waveguide instead of a single cavity located at only one of the sides of the guide.

For a more-fundamental study, a broader-band signal in the wavelength range from 1300 to 2200 nm is used to investigate miscellaneous cavity eigenmodes in this large range. Existence of three plasmonic modes is demonstrated with FDTD in a range of the 2-tuple (l, w) in the vicinity of ($l = 380$ nm, $w = 380$ nm). We are interested in the electromagnetic behaviors of the three modes. For this analysis, we start from the trajectory point ($l = 380$ nm, $w = 380$ nm). Thereafter, we modify the cavity length l around 380 nm to scan the modes from $l = 300$ to 500 nm. In this range of (l, w), we observe the evolution of the three cavity modes. Figure 7(a) shows the transmission spectrum for $l = 300$ nm with a constant w equal to 380 nm. We name '1', '2' and '3', the lower, medium and higher modes, respectively. The resonance frequencies, deduced from the dips in the transmission coefficient (figure 7(a)) are shown in figure 7(b) as a function of l. The three modes can be distinguished between each other by their characteristics: (i) localization of mode 1 along the corners of the cavity, (ii) large sides for mode 2 and (iii) small sides for mode 3. An example of the TM maps for the three modes is presented in figure 7(c) with ($l = 340$ nm, $w = 380$ nm). We note that mode 1 is symmetric with respect to the axes parallel to both small and large sides of the cavity. Mode 2 is symmetric if we consider the axis parallel to the large side of the cavity but antisymmetric with respect to the axis parallel to its small side. In contrast to mode 2, mode 3 is antisymmetric after comparison with the axis parallel to the large side of the cavity but symmetric with respect to the axis parallel to its small side. In figure 7(b), the wavelength of mode 2 increases quasi linearly when l increases from 300 to 380 nm. Thereafter, when l exceeds 380 nm, we observe an almost constant behavior or small decrease. A complementary behavior is obtained for mode 3 when the wavelength λ changes slightly for l below 380 nm while λ increases if l exceeds 380 nm. In contrast to modes 2 and 3, the resonance wavelength of mode 1 increases almost linearly when l is increased from 300 to 500 nm.

The rejection filter proposed in this section shows a significant improvement in quality factor, isolation and size lowering compared with other recent investigations. For instance,

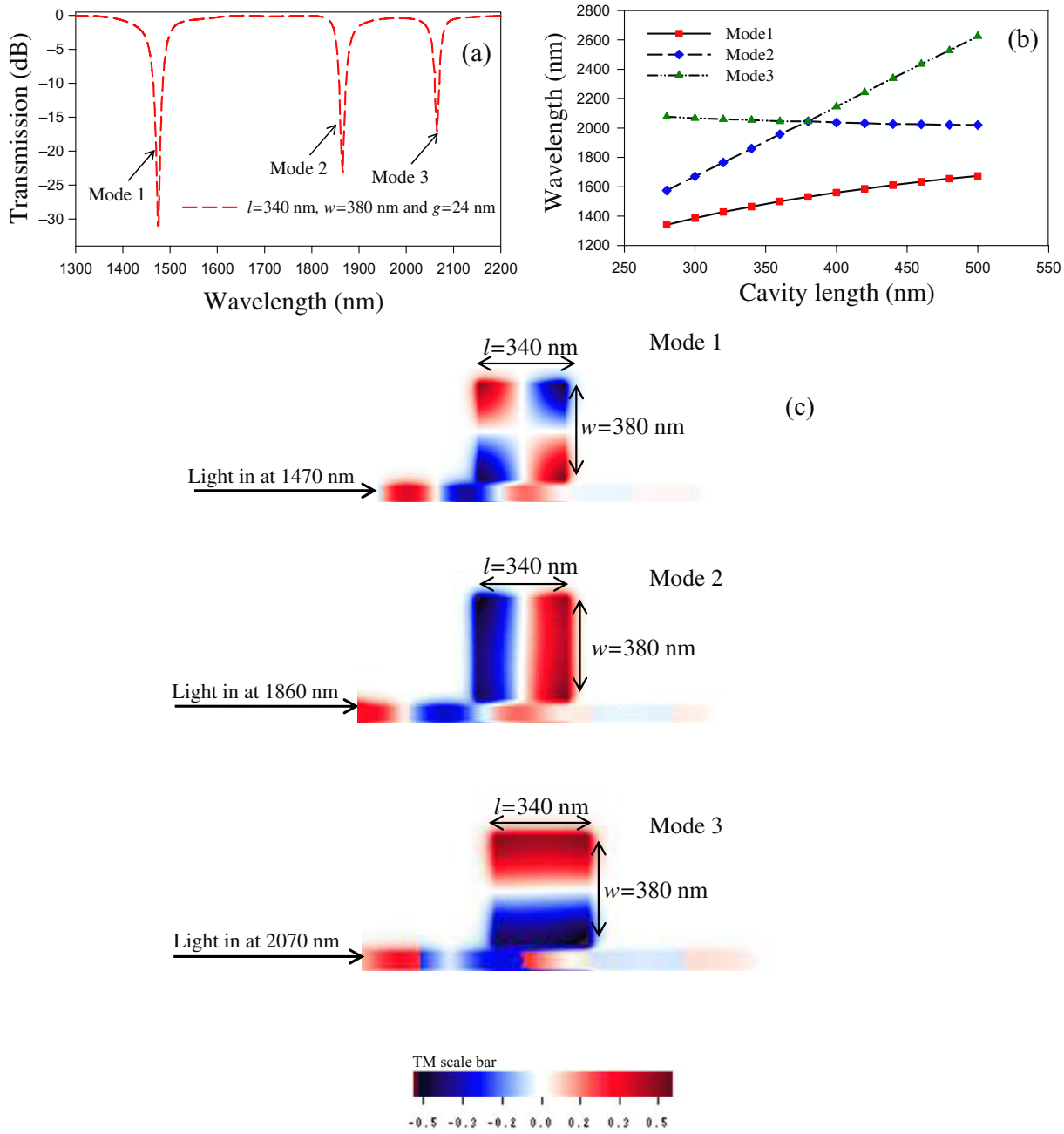

Figure 7. (a) Transmission spectra versus wavelength, given for three different SPP eigenmodes, for a cavity located on the side of the waveguide branch with $l = 340\,\text{nm}$, $w = 380\,\text{nm}$ and $g = 24\,\text{nm}$. (b) Wavelength of the maximal dips in the transmission spectra versus l for constant $w = 380\,\text{nm}$ and $g = 24\,\text{nm}$. Squares (red), diamonds (blue) and triangles (green) correspond to modes 1, 2 and 3 (respectively). (c) Magnetic-field maps (TM) for monochromatic incident radiations at the wavelengths of the zeros of the transmission coefficient (with the respective values $\lambda = 1470\,\text{nm}$, $\lambda = 1860\,\text{nm}$ and $\lambda = 2070\,\text{nm}$ for modes 1, 2 and 3).

a nanocavity resonator formed by a square ring on the side of a MIM waveguide was presented in [39]. However, the proposed ring fills an area up to 10 folds larger than that of our rectangular nanocavity. Moreover, these authors also computed dips in the transmission spectrum for resonance wavelengths from 910 to 1050 nm with isolation between −9 and −24 dB. These values are not optimized for optical telecommunication. Indeed, the wavelength range is not broad enough with a maximum λ-value of only 1200 nm. Isolation should as well be improved. Differently, we obtain dips with a good isolation down to −30 dB. In another recent example in [37], the authors proposed a rectangular nanocavity filled by air instead of SiO_2 inside Ag with a similar size than ours. From their numerical calculations, they however obtained a quality factor Q of only 21 for a metallic-gap size $g = 40$ nm while we compute in this paper $Q = 153$ (≈ 7 folds higher) for the same g value and isolation of −20 dB. As discussed in the next section, our nanocavity can also be introduced in a Y-bent add/drop connector, which was not shown in [37, 38, 40].

5. Y-bent add/drop plasmonic waveguide

In this section, we propose a 2D Y-bent plasmonic demultiplexer using the sub-waveguides detailed in sections 3 and 4 to design its two end branches. Our aim is to select (add) or reject (drop), at the same time, two different wavelengths at each output branch of the Y plasmonic add/drop device from a broadband incident signal in the range of 1100 to 2200 nm. In figure 8(a), we present the setup of the bare Y-shaped waveguide, where d is the thickness of the input sub-waveguide and output branches and D is the separation distance between the two end branches. The value of d is equal to 50 nm as that of the linear sub-waveguides studied in sections 3 and 4. D is taken equal to the small value of 400 nm. The latter values of d and D are interesting for integrated plasmonic devices at the nanoscale operating in the telecommunication range. Figure 8(b) shows the corresponding transmission spectrum probed at the right end of the two end branches of the bare guide (port 1 and port 2). Separation of the incident signal into two beams through the output branches of the Y junction does not significantly change the quality of the signals collected at the two end ports. The comparison of the sum of energy of the two signals collected on each end branch to the energy of a signal transmitted through a linear waveguide with the same width and propagation length (4.5 μm) shows a quasi zero bend loss of energy. As a result, the nanoscale Y-shaped plasmonic waveguide might be considered as a promising device for networking and all-optical nano-circuits.

In section 3, we showed that coupling of a nanoscale linear waveguide with an inside nanocavity provides a selective filtering. From this result, we study coupling of the Y device with respect to a pair of rectangular nanocavities inserted inside each output branch. Figure 9(a) represents the geometry of this structure. Denote l_1 as the length of cavity 1 located inside the lower branch and l_2 as that of cavity 2 inserted on the upper branch of the Y connector. We use the following sets of values of 440, 480 and 500 nm for l_1 and 512, 540 nm for l_2. The width w of both cavities is a constant equal to 100 nm for all analyses. Figure 9(b) shows the transmission spectrum recorded at the right-hand side of each end branch of the main guide with $l_1 = 440$ nm and $l_2 = 512$ nm in the wavelength range from 1.2 to 1.9 μm. This figure presents also the two cases when ($l_1 = 480$ nm, $l_2 = 540$ nm) and ($l_1 = 500$ nm, $l_2 = 540$ nm). We observe that, on both end branches of the Y waveguide, all wavelengths are reflected except those associated to excitation of the cavities' eigenmodes. For cavity 1 with the length $l_1 = 440$ nm (lower branch) the wavelength of the resonance mode, which is transmitted to the end part of the guide, is

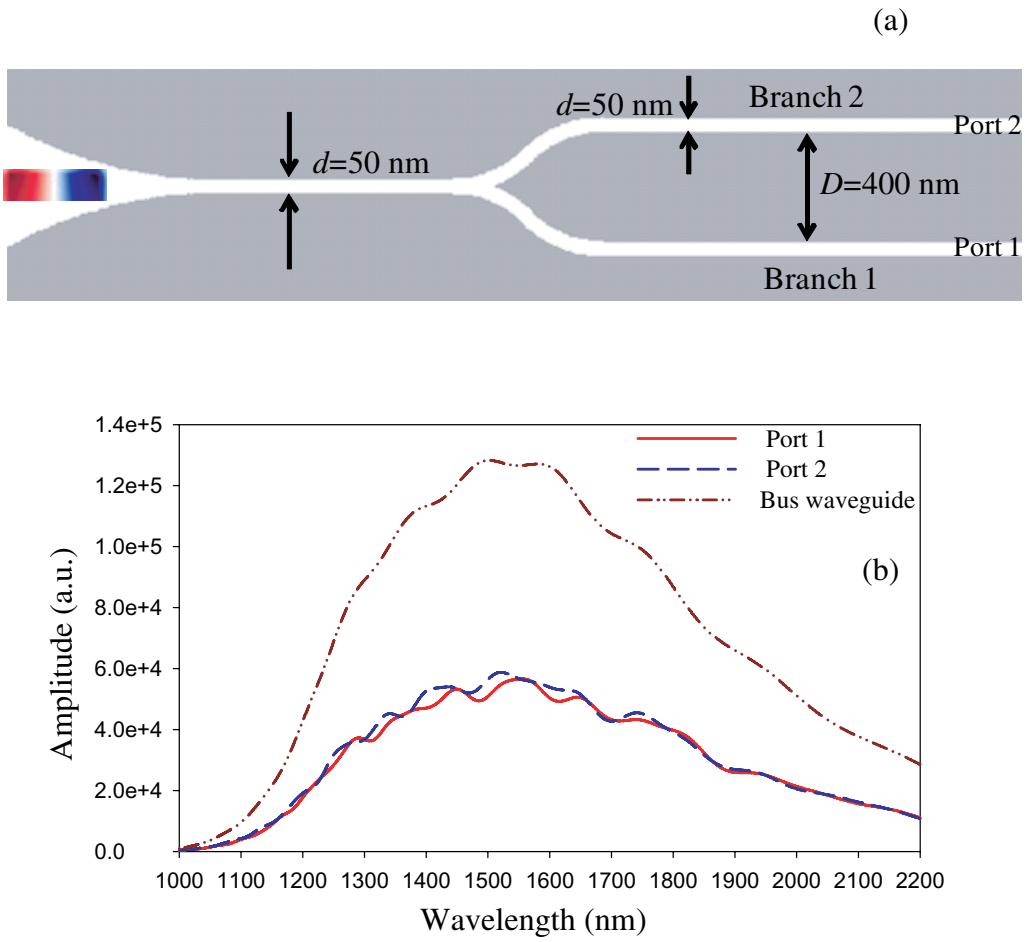

Figure 8. (a) Schematics of a bare 2D Y-bent plasmonic waveguide. The branch width is denoted by $d = 50$ nm while $D = 400$ nm is the distance between the two output branches. (b) Transmission spectrum probed at the right end of the two branches (port 1 and port 2) of the bare Y-waveguide.

equal to 1340 nm. The resonance wavelength for cavity 2 (upper branch) is equal to 1550 nm. The transmission coefficient shows that the resonance peak collected at the lower branch is transmitted by cavity 1 with an energy rate equal to 79% (i.e. −4 dB). For the resonance peak transmitted by the upper cavity (cavity 2), 64% of transmission is observed. As discussed in section 3, the filtered frequencies can be tuned in the analyzed range for specific applications by choosing appropriately the lengths of the cavities. Indeed in figure 9(b), we show the possible tuning of the two selected wavelengths by further calculating the transmission coefficients for ($l_1 = 480$ nm, $l_2 = 540$ nm) and ($l_1 = 500$ nm, $l_2 = 540$ nm), respectively. Obviously the width w of the cavities could be modified as well rather than their lengths to modify the filtered frequencies (figure 3(b)). However, to remain at the nanoscale, we keep the side dimensions of the cavities as small as possible. Also note that good performance of the device is conditioned by keeping the cavities inside the Y waveguide at a certain landmark distance of at least 1.5 μm (according to numerical tests) from the beginning of the input port. Otherwise the cavities are strongly coupled through the Y structure. In this case, we observe in the transmission

coefficient spectrum that the peaks transmitted to the right-hand side ports of each end branch are duplicated. The presented results are obtained for a distance between cavities and Y-junction equal to 2.25 μm (figure 9(b)). As explained in the precedent, the quality factor could be also improved by increasing the thickness of the two pieces of metal (metallic gap g) that separate the cavities from the Y waveguide. Figure 9(c) presents the TM map for the two resonance modes (at 1340 nm for cavity 1 and at 1550 nm for cavity 2). It shows that an incident monochromatic signal at 1340 nm interacts strongly with cavity 1 and is transmitted resonantly to the right-hand side port of the lower end branch. On the upper branch, this plane wave is reflected. Figure 9(c) also shows that an incident monochromatic signal with the wavelength of 1550 nm excites the cavity 2 eigenmode and is transmitted to the upper port. In the lower end branch, this wavelength is reflected to the entrance of the Y junction.

Finally, we study the coupling of the Y-shaped waveguide to a pair of cavities located in the outside vicinity of each end branch of the connector (see section 4). Figure 10(a) presents the structure setup. All size parameters as d and D remains equal to the values given in the preceding case ($d = 50$ nm and $D = 400$ nm). We also refer the cavities dimensions as l_1 for the length of the cavity on the side of the lower branch and l_2 for the length of the cavity on the side of the upper branch of the Y waveguide. The cavity width remains denoted w and equal to 100 nm for both lower and upper cavities. In figure 10(b), we display the corresponding transmission spectrum when $l_1 = 440$ nm and $l_2 = 512$ nm for a metallic gap $g = 36$ nm. Interaction between the cavity and incident signal on the lower end branch through the metallic gap creates a -28 dB dip at the wavelength of 1350 nm in the transmission spectrum. This wavelength is quite similar to that obtained for a peak when the cavity is located inside the end branch. In the upper end branch of the connector, the interaction between the cavity and incident signal generates a -22 dB dip at the wavelength of 1560 nm in the transmission spectrum. This wavelength is identical to the resonance-mode wavelength when the cavity is inside the upper end branch of the Y junction. We notice tiny disturbances on the transmission spectrum. Especially, transmission exceeds 0 dB around the reflected frequencies. This can be due to the following effects: when the resonance wavelength of cavity 1 (lower end branch) is reflected towards the entrance of the Y junction, a secondary beam at this λ value goes up to the upper end branch of the waveguide. This reflection leads to an additional small quantity of energy (with respect to the incident energy) at this wavelength in the upper end branch of the connector. The same phenomenon explains the higher value than 0 dB in the transmission spectrum around the other resonance mode wavelength (cavity 2). However, these additional energies at the resonance wavelengths are low (only 4 dB) and do not disturb the reflected frequencies. We also present the transmission coefficient for the case when $l_1 = 460$ nm and $l_2 = 540$ nm whose resonance mode wavelengths are respectively 1400 nm (with -27 dB dip in the transmission) and 1600 nm (with -29 dB dip in the transmission). This analysis demonstrates the possibility of tuning the reflected frequencies in the telecommunication range for potential applications. Remind that performance of the device is correlated to the distance between the cavities and beginning of the Y junction. Indeed, this distance should be at least equal to 1.5 μm (according to numerical tests). Otherwise, the cavities are strongly coupled and a non-negligible disturbance appears in the transmission spectrum, which can lead to duplication of the reflected frequencies. As for cavities inserted inside the end branches of the Y-shaped waveguide, this distance is set to 2.25 μm. As mentioned before, the quality factor in the double-rejection Y connector can also be improved by increasing the metallic gap size g. The magnetic-field maps for the reflected wavelengths are presented in figure 10(c). They show a strong coupling between the incident

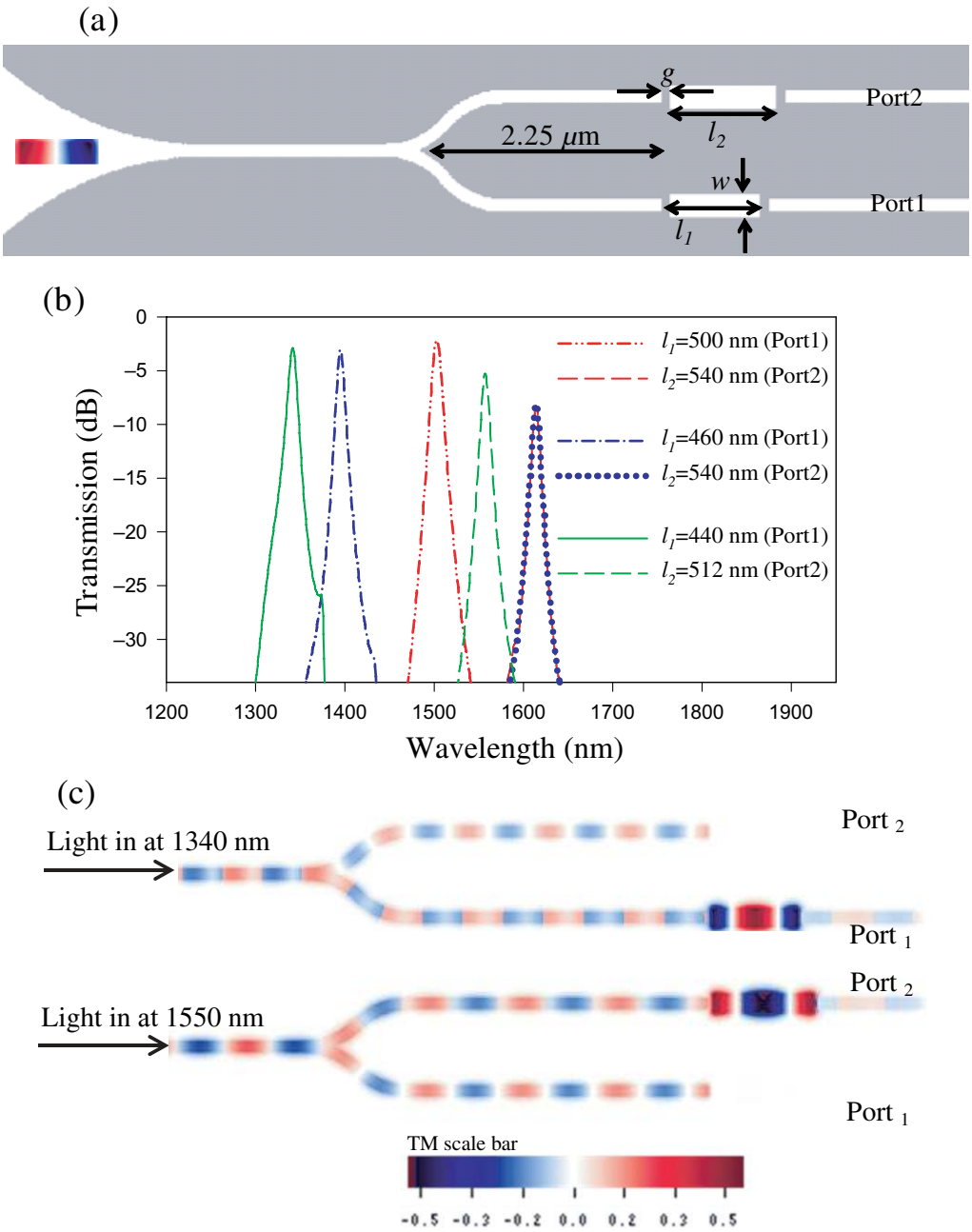

Figure 9. (a) Schematics of a Y-bent waveguide coupled to a pair of rectangular nanocavities inside each of its output branches with the widths l_1 and l_2 for the lower and upper cavities, respectively. (b) Transmission spectrum versus wavelength for the Y-bent system shown in (a) using the length parameters $l_1 = 440$, 460 and 500 nm for the lower inside cavity and $l_2 = 512$ and 540 nm for the upper inside cavity. The constant width w is equal to 100 nm for both cavities. (c) Magnetic-field maps (TM) for monochromatic incident signals at the wavelengths of the maxima of the transmission coefficient ($\lambda = 1340$ nm for the resonance mode of the lower cavity and $\lambda = 1550$ nm for that of the upper cavity).

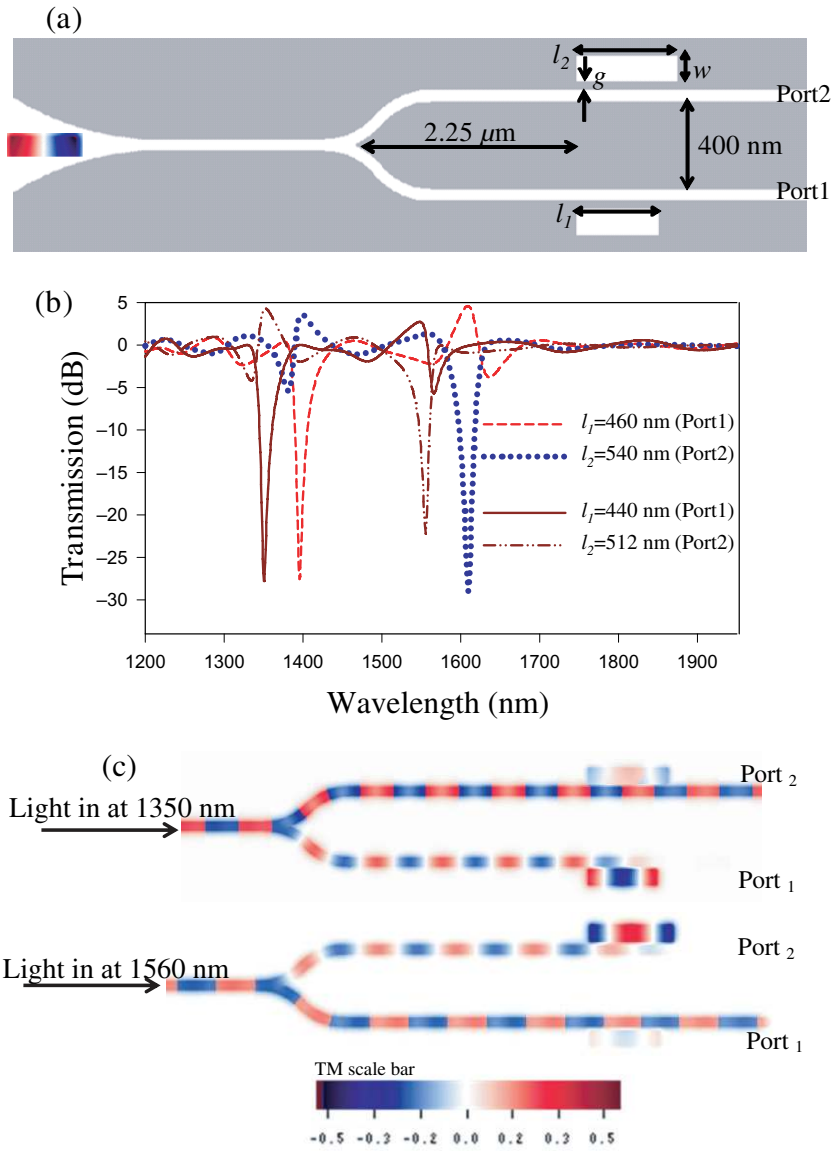

Figure 10. (a) Schematics of a 2D Y-bent plasmonic waveguide coupled to a pair of rectangular nanocavities placed on the side of its upper and lower branches. (b) Transmission spectrum versus wavelength at ports 1 and 2 for the system depicted in (a) where $l_1 = 440$ and 460 nm are the values used for the length of the lower cavity while $l_2 = 512$ and 540 nm are used for that of the upper cavity. The constant width w of both cavities is equal to 100 nm. (c) Magnetic-field maps (TM) for monochromatic incident signals at the wavelengths of the zeros of the transmission coefficient ($\lambda = 1350$ nm for the resonance mode of the lower cavity and $\lambda = 1560$ nm for that of the upper cavity). The utilized length of the lower cavity is $l_1 = 440$ nm while that of the upper cavity is $l_2 = 512$ nm.

frequencies and cavities (located on the side of the upper or lower end branches), which leads to their reflection by one of the end branches and transmission by the other.

Owing to its sub-waveguide width of only 50 nm and distance of 400 nm between its end branches, which is small compared to preceding studies of other plasmonic devices, the proposed plasmonic Y-bent demultiplexer might become a component of choice for the design of all-optical integrated architectures for optical networking and computing, e.g. at the nanoscale using the usual telecommunication wavelengths. For instance, we were able in this work to decrease by 625 folds the distance between the sub-waveguides with respect to that utilized in [41].

6. Conclusion

We firstly reported on numerical investigations of the transmission through a nanoscale plasmonic linear waveguide in the telecommunication range (around 1.55 μm) coupled to a single SiO_2 cavity located either inside or on the side of the main branch that is sandwiched between two Ag parts. We show the possible design of selective or rejection filters (respectively) for the SPP cavity modes. We especially emphasize the corresponding peak or dip in the transmission spectrum. The filtered frequency can be tuned from an appropriate choice of the size parameters. These filtering properties are proposed to design a nanoscale plasmonic demultiplexer based on a Y-bent add/drop waveguide operating around 1550 nm either in selection (add) or reflection (drop) of two different wavelengths received in the lower and upper output branches. Possible tuning of the two selected or reflected wavelengths at the same time is shown by modification of the dimensions of both cavities. Our Y-bent waveguide is numerically designed with smaller size parameters than those used in preceding studies of other plasmonic components. Moreover, we obtain high quality factors and good isolation of the rejected zeros in agreement with optical telecommunication. The small dimensions of our add/drop Y connector might be an advantage to fabricate all-optical integrated devices and circuits at the nanoscale with operation wavelengths in the usual telecommunication range given by silicon dioxide. Finally, note that the same concept was used by the same authors [38] to discuss the possibility of selective or rejective resonances in the range of the visible wavelengths.

References

[1] Barnes W L, Dereux A and Ebbesen T W 2003 *Nature* **424** 824
[2] Miyazaki H T and Kurokawa Y 2006 *Phys. Rev. Lett.* **96** 097401
[3] Berini P 2000 *Phys. Rev.* B **61** 10484
[4] Berini P 2008 *New J. Phys.* **10** 105010
[5] Pile D F P and Gramotnev D K 2005 *Appl. Phys. Lett.* **30** 1186
[6] Bozhevolnyi S I, Volkov V S, Devaux E and Ebbesen T W 2005 *Phys. Rev. Lett.* **95** 046802
[7] Bozhevolnyi S I, Volkov V S, Devaux E, Laluet J Y and Ebbesen T W 2006 *Nature* **440** 508
[8] Arbel D and Orenstein M 2008 *Opt. Express.* **16** 3114
[9] Dionne J A, Sweatlock L A, Atwater H A and Polman A 2005 *Phys. Rev.* B **72** 075405
[10] Liu I, Han Z and He S 2005 *Opt. Express.* **13** 6645
[11] Han Z, Van V, Herman W N and Ho P-T 2009 *Opt. Express* **17** 12678
[12] Pile D F P, Ogawa T, Gramotnev D K, Matsuzaki Y, Vernon K C, Yamaguchi K, Okamoto T, Haraguchi M and Fukui M 2005 *Appl. Phys. Lett.* **87** 261114
[13] Moreno E, Rodrigo S G, Bozhevolnyi S I, Moreno L M and Vidal F G 2008 *Phys. Rev. Lett.* **100** 023901

[14] Boltasseva A, Volkov S V, Nielsen B R, Moreno E, Rodrigo S G and Bozhevolnyi S I 2008 *Opt. Express* **16** 5252
[15] Oulton R F, Bartal G, Pile D F P and Zhang X 2008 *New J. Phys.* **10** 105018
[16] Søndergaard T, Jung J, Bozhevolnyi S I and Della Valle G 2008 *New J. Phys.* **10** 105008
[17] Dionne J A, Sweatlock L A, Atwater H A and Polman A 2006 *Phys. Rev.* B **73** 035407
[18] Neutens P, Dorpe P V, Vlaminck L D, Lagae L and Borghs G 2009 *Nat. Photon.* **3** 283
[19] Yu Z, Veronis G, Fan S and Brongersma M L 2008 *Appl. Phys. Lett.* **92** 041117–9
[20] Min C and Veronis G 2009 *Opt. Express* **17** 10757
[21] Wu X, Zhang J and Gong Q 2009 *Opt. Express* **17** 2818
[22] Hang Y C, Wang C-M, Abbas M N, Shih M-H and Tsai D P 2009 *Opt. Express* **17** 13526
[23] Gómez Rivas J, Vecchi G and Giannini V 2008 *New J. Phys.* **10** 105007
[24] Gong Y, Wang L, Hu X, Li X and Liu X 2009 *Opt. Express* **17** 13727
[25] Ahn K J, Lee K G, Kihm H W, Seo M A, Adam A J L, Planken P C M and Kim D S 2008 *New J. Phys.* **10** 105003
[26] Taminiau T H, Stefani F D and van Hulst N F 2008 *New J. Phys.* **10** 105005
[27] Mohammadi A, Sandoghdar V and Agio M 2008 *New J. Phys.* **10** 105015
[28] Taflove A 2000 *Computational Electrodynamics: The Finite Difference Time Domain Method* 2nd edn (Norwood: Artech House)
[29] Wang C M, Huang H I, Chao C C, Chang J Y and Sheng Y 2007 *Opt. Express* **15** 3496
[30] Xiao S, Liu L and Qiu M 2006 *Opt. Express* **14** 2932
[31] Veronis G and Fan S 2007 *Opt. Express* **15** 1211
[32] Johnson P and Christy R 1972 *Phys. Rev.* B **6** 4370–9
[33] Kurokawa Y and Miyazaki H T 2007 *Phys. Rev.* B **75** 035411
[34] Kottmann J P, Martin O J F, Smith D R and Schultz S 2001 *Phys. Rev.* B **64** 235403
[35] Esaki L 1989 Proc. 3rd Int. Symp. Foundations of Quantum Mechanics (Tokyo) pp 369–82
[36] Zianni X 2008 *Phys. Rev.* B **78** 165327
[37] Zhang Q, Huang X-G, Lin X-S, Tao J and Jin X-P 2009 *Opt. Express* **17** 7549
[38] Noual A, Pennec Y, Akjouj A, Djafari-Rouhani B and Dobrzynski L 2009 *J. Phys.: Condens. Matter.* **21** 375301
[39] Khelif A, Djafari-Rouhani B, Vasseur J O and Deymier P A 2003 *Phys. Rev.* B **68** 024302
[40] Hosseini A and Massoud Y 2007 *Appl. Phys. Lett.* **90** 181102
[41] Charbonneau R, Lahoud N, Mattiussi G and Berini P 2005 *Opt. Express* **13** 977